High Power Laser Science and Engineering (2013), *vol.* 1(2), 74–79.

doi: 10.1017/hpl.2013.12

Upper-limit power for self-guided propagation of intense lasers in underdense plasma

Wei-Min Wang[1], Zheng-Ming Sheng[1,2], Yu-Tong Li[1], and Jie Zhang[1,2]

[1]*Beijing National Laboratory for Condensed Matter Physics, Institute of Physics, CAS, Beijing 100190, China*

[2]*Key Laboratory for Laser Plasmas (Ministry of Education) and Department of Physics, Shanghai Jiao Tong University, Shanghai 200240, China*

(*Received 12 September 2012; revised 7 November 2012; accepted 25 April 2013*)

Abstract

It is found that there is an upper-limit critical power for self-guided propagation of intense lasers in plasma in addition to the well-known lower-limit critical power set by the relativistic effect. Above this upper-limit critical power, the laser pulse experiences defocusing due to expulsion of local plasma electrons by the transverse ponderomotive force. Associated with the upper-limit power, a lower-limit critical plasma density is also found for a given laser spot size, below which self-focusing does not occur for any laser power. Both the upper-limit power and the lower-limit density are derived theoretically and verified by two-dimensional particle-in-cell simulations. The present study provides new guidance for experimental designs, where self-guided propagation of lasers is essential.

Keywords: laser plasma interaction; laser wakefield acceleration; particle-in-cell; self-focusing

1. Introduction

Laser propagation in plasma is a fundamental and important issue in laser plasma interactions, which is related to a number of applications such as the fast ignition scheme for inertial confinement fusion [1,2], the laser wakefield acceleration of electrons [3–8], and lightning channeling in air [9,10]. Usually, these applications require that intense laser pulses can stably propagate over a large distance in plasma. On this issue, many theoretical and experimental studies have been performed in the last 30 years [11–24]. Self-focusing of an ultrashort intense laser pulse in a tenuous plasma was investigated theoretically in Refs. [11–15], and the well-known critical laser power $P_c = 17(n_c/n_e)$ GW required for self-focusing was found [13,14], where n_e is the plasma electron density, $n_c = m\omega^2/4\pi e^2$ is the critical density, and ω is the laser frequency. Since then, there have been a lot of studies on this topic when the laser power is around P_c, e.g., laser channeling in underdense plasmas [16–18], laser guiding in plasma channels [19,20], and propagation of multi-laser beams in plasmas [21–24].

Meanwhile, ultrashort ultraintense laser technology has been developing quickly. A few Petawatt (PW) laser systems are available nowadays [25]. The extreme light infrastructure (ELI) will be able to provide hundredsof PW laser beams with intensity as high as 10^{22}–10^{25} Wcm^{-2}. In this case, the laser power will be much higher than P_c. It is interesting to investigate how such laser pulses can stably be self-guided. Actually, there have been a lot of laser wakefield acceleration (LWFA) experiments conducted with laser power about 10 P_c for 1 GeV-scale electron beam generation [26–29].

In this paper, we focus on the propagation of extremely high power lasers. It is shown that there is an upper-limit power for self-guided propagation of laser pulses in underdense plasma. This is caused by the transverse ponderomotive force of the laser pulses, expelling local plasma electrons and creating an electron-free channel in a certain area. This effect can lead to defocused propagation of the laser pulses similar to in the vacuum, which may already occur at tens of P_c. Here, we call such a phenomenon *ponderomotive defocusing*, which suggests that ponderomotive forces may not help laser self-focusing in a high laser power regime.

The outline of the paper is as follows. First, the ponderomotive defocusing is demonstrated through a set of two-dimensional (2D) particle-in-cell (PIC) simulations in Section 2. Then both the upper-limit critical laser power and the lower-limit critical plasma density for self-focusing are derived theoretically in Section 3. The results are checked by 2D PIC simulations in Section 4. Finally, the paper is summarized in Section 5. It should be noted that ponderomotive defocusing has been demonstrated in our paper [30] by three-dimensional PIC simulations and the upper-limit

Correspondence to: Wei-Min Wang, Institute of Physics, CAS, P. O. Box 603(33), Beijing 100190, China. Email: hbwwm1@iphy.ac.cn

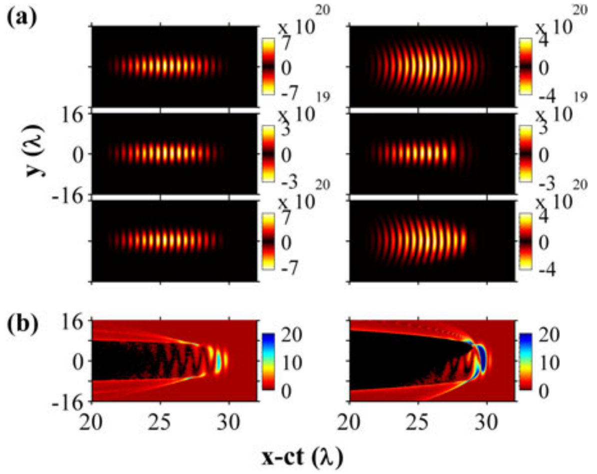

Figure 1. (a) Spacial distributions of the laser intensities with $r_0 = 4\ \lambda$. The first and second columns are the results when the lasers propagate for the distances of 0.5 and 2 x_R, respectively. The first row shows that the laser of 219 TW propagates in the vacuum. The second and third rows show the propagation of the laser pulses with powers of 10 P_c (8.8 TW) and 250 $P_c = 10\ P_u$ (219 TW), respectively, in the plasma with density $0.014 n_c = 5\ n_L$. (b) Spacial distributions of the electron densities normalized by n_L after the propagation of 0.5 x_R, where the initial electron densities are taken as 5 n_L and laser pulses with powers of 10 P_u and 100 P_u are taken in the first and second columns.

critical laser power has been derived. In the current paper, we will present a more detailed investigation by 2D PIC simulations and give a more detailed derivation of the upper-limit power.

2. Simulation demonstration of ponderomotive defocusing

We first demonstrate the ponderomotive defocusing by the results of a set of 2D PIC simulations, shown in Figure 1(a) (a similar 3D PIC demonstration can be seen in [30]). In the simulations, 1 μm wavelength laser pulses propagate along the $+x$ direction. They are linearly polarized along the y direction and their vector potential takes the form

$$A_y = a_0 \sin\left(\frac{\pi\xi}{\tau_0}\right) \sin(2\pi\xi) \exp\left(\frac{-y^2}{r_0^2}\right), \quad 0 \leqslant \xi < \tau_0, \tag{1}$$

where $\xi = t - x$, t, and x are normalized by the laser period T and wavelength λ, a_0 is normalized by $m_e c^2/e$, and c is the speed of light in the vacuum. We take the laser duration $\tau_0 = 10\ \lambda$ and spot radius $r_0 = 4\ \lambda$. Plasma with the uniform density of $n_e = 0.014\ n_c$ or $5\ n_L$ [n_L is a lower-limit density defined by Equation (14)] is taken in the second and third rows in Figure 1, where $n_c = 1.1 \times 10^{21}\ \text{cm}^{-3}$. In the simulations, we take a moving window with size 32 λ in the x direction.

Figure 1(a) shows the spacial distributions of the laser electric fields at propagation distances of 0.25 and 2 x_R, respectively, where $x_R = \pi r_0^2/\lambda$ is the Rayleigh length. It is shown in the second row that the laser pulse with the power of 10 P_c(8.8 TW) propagates with self-focusing for several x_R in the plasma. However, when the laser power is increased to 250 $P_c = 10\ P_u$ (219 TW) [P_u is an upper-limit power defined by Equation (13)], self-focusing does not appear, and the evolution of the laser pulse is very close to that in the vacuum, as observed in the first and third rows. We call this phenomenon ponderomotive defocusing in a plasma. This has resulted from the complete expulsion of all local electrons by the transverse ponderomotive force of the extremely intense laser pulse, as shown in the first picture in Figure 1(b). Therefore, the laser propagates as in the vacuum.

3. Upper-limit laser power and lower-limit plasma density

One expects that there is a laser power threshold above which the laser pulse starts to experience ponderomotive defocusing in a plasma. This threshold can be given according to balance of the transverse ponderomotive force with the electrostatic (ES) force. The ES force is formed by charge separation resulting from expulsion of local plasma electrons by the transverse ponderomotive force. The ES force counterworks the transverse ponderomotive one, which prevents ponderomotive defocusing. One can assume that the ES force is equal to the transverse ponderomotive one at some radius r and that the plasma electrons are completely expelled within the column with radius r. If r is smaller than the laser spot radius r_0, one can consider that the ES force is able to succeed in preventing the occurrence of ponderomotive defocusing. Then, one can find the laser power threshold for ponderomotive defocusing through the conditions of balance of the ES force with the ponderomotive one at r_0.

In the following, we derive this power threshold. For this purpose, one needs to derive the ponderomotive force in a highly relativistic case. Note that the ponderomotive force have been derived in weak and moderate relativistic cases with the electron longitudinal velocity not so close to c[12,14,20,35,36]. Here, we try to derive the ponderomotive force expressed approximately by the laser parameters in a highly relativistic case, where the longitudinal electron momentum may be much larger than the transverse one. Set that the laser pulse propagates along the $+x$ direction and has linear polarization along the y direction, with the vector potential

$$\mathbf{A} = \hat{\mathbf{e}}_y a_0 \sin\left(\frac{\pi\xi}{\tau_0}\right) \sin(2\pi\xi) \exp\left(\frac{-r^2}{r_0^2}\right), \quad 0 \leqslant \xi < \tau_0. \tag{2}$$

Under the laser field, the motion of an electron in a plasma is governed by the Hamiltonian [31,32]:

$$H = \gamma - \phi, \tag{3}$$

https://doi.org/10.1017/hpl.2013.12 Published online by Cambridge University Press

where ϕ is the scalar potential normalized by $m_e c^2/e$, $\gamma = \sqrt{1+\mathbf{p}^2}$ is the relativistic factor, $\mathbf{p}$ is the momentum normalized by $m_e c$, and the general momentum $\mathbf{P} = \mathbf{p} - \mathbf{A}$. Taking the partial derivative of H with respect to transverse coordinates (marked by $\perp$), one can obtain the transverse motion equation of the electron:

$$\frac{d(\mathbf{p}_\perp - \mathbf{A})}{dt} = -\nabla_\perp(\gamma - \phi), \tag{4}$$

where the first term on the right-hand side is the transverse ponderomotive force and the second is the transverse ES force. The longitudinal motion equation is given by

$$\frac{dp_x}{dt} = -\frac{\partial(\gamma - \phi)}{\partial x}, \tag{5}$$

through taking the partial derivative of H with respect to x. Here, a tenuous plasma is considered, and therefore the laser frequency ω is much higher than the plasma oscillation frequency $\omega_p = \sqrt{4\pi e^2 n_e/m_e}$. As a result, one can assume that every quantity Q can be divided into a fast varying part and slowly varying part, i.e., $Q = Q^f + Q^s$, where Q^f varies at the order of ω and Q^s varies at the order of ω_p. The fast varying parts of Equation (4) satisfy

$$\frac{d(\mathbf{p}^f_\perp - \mathbf{A})}{dt} = 0. \tag{6}$$

We have assumed that the contribution of the transverse ponderomotive force on the fast varying momentum is much smaller than the laser field since the transverse ponderomotive force expels the electron mostly outwards. The slowly varying parts satisfy

$$\frac{d\langle \mathbf{p}_\perp\rangle}{dt} = -\langle \nabla_\perp \gamma\rangle + \nabla_\perp \phi, \tag{7}$$

where we have defined $\langle Q\rangle = \int_0^T Q dt/T$, and T is the laser period. The fast varying parts of Equation (5) are given by

$$\frac{dp^f_x}{dt} = -\frac{\partial \gamma^f}{\partial x}. \tag{8}$$

According to Equations (6) and (8), one can construct a fast varying Hamiltonian $H^f = \gamma^f$. Consider that in a tenuous plasma $\mathbf{A}$, and then H^f is the function of $\xi = t - x$ for a given electron, since the time of interaction of the electron with the laser pulse is at the order of the laser duration usually, within which the laser waveform does not vary much. Then one can obtain a conversed quantity $H^f - p^f_x$, which gives $\gamma^f - p^f_x = 1$. It can be easily obtained that [31,32] $\mathbf{p}^f_\perp = \mathbf{A}$, $p^f_x = \mathbf{A}^2/2$, and $\gamma^f = 1 + \mathbf{A}^2/2$. To give the transverse ponderomotive force $\mathbf{F}_p = -\langle \nabla_\perp \gamma\rangle$, one needs to get the slowly varying momentum $\langle \mathbf{p}\rangle$, which is very difficult. Here, we take the 0-order approximation $\gamma \simeq \gamma^f$ assuming $p^f \gg \langle p\rangle$, insert it into the expression of $\mathbf{F}_p$, and obtain $\mathbf{F}_p \simeq -\langle \nabla_\perp \mathbf{A}^2/2\rangle$. Taking the laser vector potential as Equation (2), one can obtain the transverse ponderomotive force at the laser pulse peak ($\xi = \tau_0/2$):

$$\mathbf{F}_p \simeq \hat{\mathbf{e}}_r \frac{a_0^2 r}{r_0^2} \exp\left(\frac{-2r^2}{r_0^2}\right). \tag{9}$$

In terms of the Poisson equation, one can easily present the transverse ES force,

$$\mathbf{F}_{es} = \nabla_\perp \phi = -\hat{\mathbf{e}}_r 2\pi^2 n_e r, \tag{10}$$

if it is assumed that the plasma electrons are expelled completely within the column with the radius r and the plasma ions are moveless within the laser pulse duration. Here, the radius r is normalized by λ, and the electron density is normalized by n_c.

Through $\mathbf{F}_p(r = r_0) + \mathbf{F}_{es}(r = r_0) = 0$, one can derive $a_0^2 = 2\pi^2 n_e r_0^2 \exp(2)$. Then one can obtain the upper-limit critical power for self-focusing or the power threshold for ponderomotive defocusing:

$$P_u = \frac{n_e r_0^4}{n_c \lambda^4} \times 3.14\ \text{TW}. \tag{11}$$

Only when the laser power P_0 satisfies $P_c < P_0 < P_u$ can the laser pulse experience self-focusing. When $P_0 > P_u$, it will experience ponderomotive defocusing. Furthermore, for occurrence of self-focusing, it is required that $P_c > P_u$ or $n_e r_0^2 > 0.074\ n_c \lambda^2$. Otherwise, self-focusing cannot occur for any laser power. Hence, the lower-limit critical density n_L for self-focusing can be defined by

$$n_L = 0.074\, n_c \frac{\lambda^2}{r_0^2}. \tag{12}$$

Equations (11) and (12) indicate that the occurrence of self-focusing depends not only on the laser power and plasma electron density, but also on the laser spot size; the latter has been largely ignored.

In the 2D slab geometry, P_c is reduced by a factor $\sqrt{2}$[33,34], $\mathbf{F}_{es}$ is enhanced by a factor 2, and $\mathbf{F}_p \simeq \hat{\mathbf{e}}_r \frac{a_0^2 y}{r_0^2} \exp(-2y^2/r_0^2)$, where the laser vector potential has been taken as Equation (1). Then, one can rewrite Equations (11) and (12) in the 2D slab geometry as

$$P_u = \frac{n_e r_0^4}{n_c \lambda^4} \times 6.28\ \text{TW} \tag{13}$$

and

$$n_L = 0.044\, n_c \frac{\lambda^2}{r_0^2}. \tag{14}$$

We will check them by 2D PIC simulations below. With the help of n_L, the two critical powers P_u and P_c are related by

$$P_u = \left(\frac{n_e}{n_L}\right)^2 P_c, \tag{15}$$

which is valid for both 3D geometry and 2D slab geometry.

It should be pointed out that our model holds when the longitudinal electron momentum is important, which is jus-

https://doi.org/10.1017/hpl.2013.12 Published online by Cambridge University Press

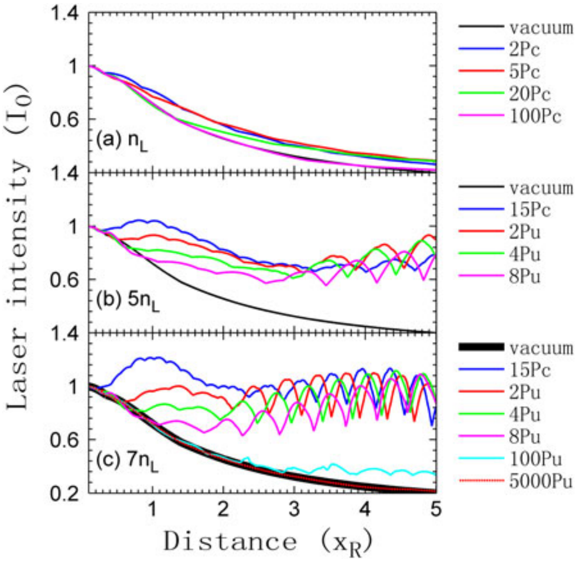

Figure 2. Evolution of the laser peak intensity with the propagation distance. Plasma densities of 1, 5 and 7 n_L are taken in (a)–(c), respectively. In every picture, the black curve corresponds to a laser propagating in the vacuum, and the other curves correspond to the lasers with different initial powers P_0 in plasmas. The laser spot radius is fixed as 8 λ.

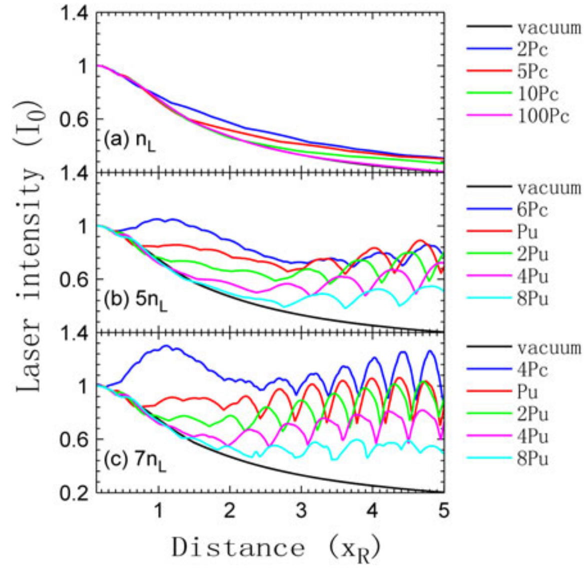

Figure 3. Evolution of the laser peak intensity with the propagation distance. Plasma densities of 1, 5 and 7 n_L are taken in (a)–(c), respectively. In every picture, the black curve corresponds to a laser propagating in the vacuum and the other curves correspond to lasers with different initial powers P_0 in plasmas. The laser spot radius is fixed as 4 λ.

tified, in particular, for an ultrashort ultraintense laser pulse. While the longitudinal electron momentum is neglected, one can assume $\gamma \simeq \sqrt{1+a_0^2}$ and derive the laser amplitude $a_0 \simeq \pi^2(n_e/n_c)(r_0^2/\lambda_0^2)$[35,36], when the ES force and the ponderomotive force are balanced at r_0. In this case, one can derive $P'_u = (n_e^2 r_0^6)/(n_c^2\lambda^6) \times 2.1$ TW and $n'_L = 0.2 n_c\lambda^2/r_0^2$ in 3D geometry, as well as in the 2D slab geometry $P'_u = (n_e^2 r_0^6)/(n_c^2\lambda^6)\times 4.2$ TW and $n'_L = 0.14 n_c\lambda^2/r_0^2$. It is obtained that $n'_L \simeq 3n_L$, and usually P'_u is smaller than P_u in the underdense plasma case. Taking the laser and plasma parameters from this Letter, one can calculate $P_u = 4P'_u \sim 7P'_u$. We will take the critical power and density as P_u and n_L because they show better agreement with the simulation results presented below.

4. Verification of the theoretic results by PIC simulations

We fix the laser spot radius r_0 at 8λ and vary the plasma density as well as the laser power. The evolution of the laser intensity with the propagation distance is plotted Figure 2. The plot with the initial plasma density $n_e = n_L$ illustrates clearly that self-focusing does not occur at any laser power. For a larger P_0, the evolution curve of the laser intensity is closer to the one in the vacuum. Notice that the curve with $100P_c$ nearly coincides with the one in the vacuum. When the plasma density is increased to $5n_L$ (with $P_u = 25P_c$), occurrence of self-focusing is observed at $15P_c$, as shown in Figure 2(b). As the power is enhanced to 2, 4 and 8 P_u, the corresponding curves at the beginning phase are close to the one in the vacuum. After a distance of defocusing, self-focusing appears because the self-focusing condition is satisfied with the reduced laser intensity and the increased laser spot radius. This distance of defocusing grows with the increase of the initial laser power. Similar results can also be seen in the plot with the plasma density of $7n_L$, although stronger self-focusing is observed at $15P_c$. In particular, when P_0 is up to 5000 P_u, the laser evolves like in the vacuum in the whole distance of 5 x_R. Here, in the simulations we judge if a laser pulse self-focuses or not according to the evolution curve at the beginning phase.

Then we take the laser spot radius as 4 and 16 λ, respectively, and the results are displayed in Figures 3 and 4. It is found that self-focusing begins to occur at the plasma densities of 5 and 6 n_L, respectively, for cases with laser spot radiuses of 4 and 16 λ; ponderomotive defocusing starts to be observed obviously at laser power of P_u and 4 P_u, respectively, for the cases with 4 and 16 λ (this value is about 2 P_u for the case with 8 λ). One can also see from Figures 2 and 3, and 4 that, for a smaller laser spot radius, the curve with the same initial laser power, which takes the unit as the respective P_c or P_u, approaches the one in the vacuum within a longer distance. These indicate that Equations (13) and (14) can better predict the threshold of ponderomotive defocusing for a smaller laser spot radius r_0. This is because, for a smaller r_0, the transverse ponderomotive force expels the electrons outside of r_0 faster and more easily, and thus the assumption is better that the electrons are completely expelled within the column with radius r_0. This can be observed from the second and third pictures in Figure 1(b).

Besides, one can see from Figure 4(c) that the laser pulses attenuate at large propagation distances due to the light

https://doi.org/10.1017/hpl.2013.12 Published online by Cambridge University Press

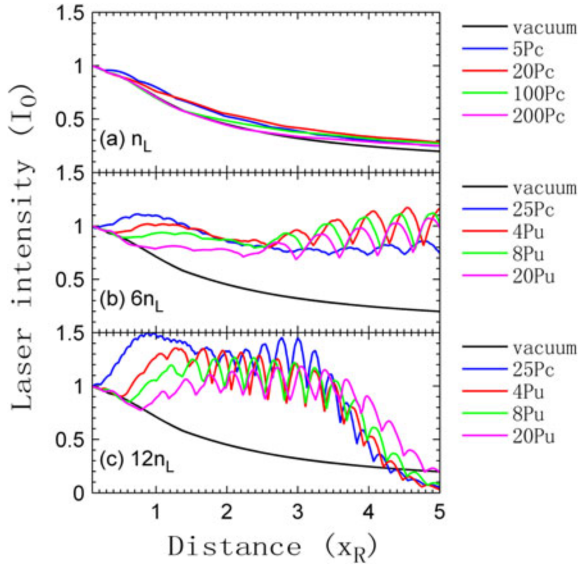

Figure 4. Evolution of the laser peak intensity with the propagation distance. Plasma densities of 1, 6 and 12 n_L are taken in (a)–(c), respectively. In every picture, the black curve corresponds to a laser propagating in the vacuum and the other curves correspond to the lasers with different initial powers P_0 in plasmas. The laser spot radius is fixed as 16 λ.

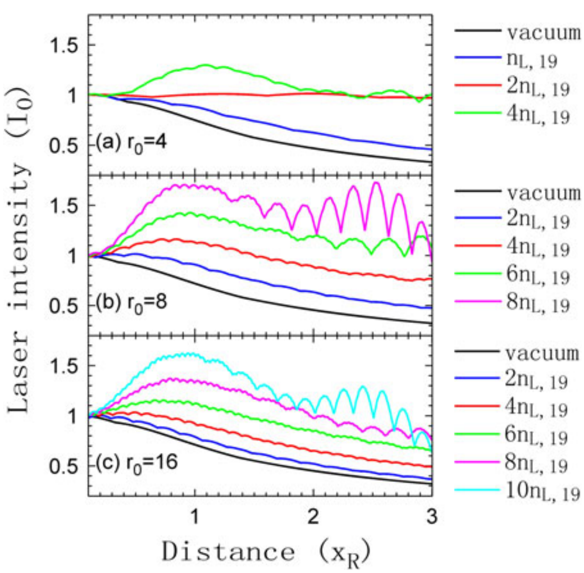

Figure 5. Evolution of the laser peak intensity with the propagation distance. Laser spot radiuses of 4, 8 and 16 λ are taken in (a)–(c), respectively. In every picture, the black curve corresponds to a laser propagating in the vacuum and the other curves correspond to lasers in the plasmas with different densities. The initial laser intensity is fixed as 10^{19} Wcm^{-2}.

absorption by the plasmas. One notices that x_R is as large as 804 λ for the laser pulse with $r_0 = 16$ λ. The light absorption effect will also becomes important when the plasma density is high, which can be observed in Figure 6.

Next, we fix the laser intensity I_0 and vary r_0 as well as the plasma density n_e to check Equations (13) and (14)

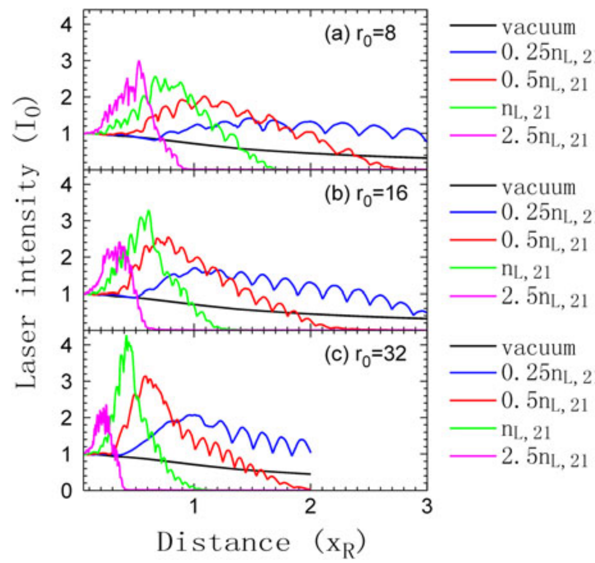

Figure 6. Evolution of the laser peak intensity with the propagation distance. Laser spot radiuses of 8, 16 and 32 λ are taken in (a)–(c), respectively. In every picture, the black curve corresponds to a laser propagating in the vacuum and the other curves correspond to lasers in the plasmas with different densities. The initial laser intensity is fixed as 10^{21} Wcm^{-2}.

in another way. As mentioned above, $P_c \leqslant P_0 \leqslant P_u$ is required for self-focusing. When $I_0 = 10^{19}$ Wcm^{-2}, this gives that $n_e \geqslant n_{L,19} = 0.077 n_c(\lambda^2/r_0^2) = 1.8 n_L$ according to Equations (13) and (14). This prediction is confirmed by Figure 5. For $r_0 = 4\lambda$, self-focusing begins to occur at $n_e = 2n_{L,19}$; for $r_0 = 8\lambda$, it begins at $4n_{L,19}$; for $r_0 = 16\lambda$, it begins at $6n_{L,19}$. For a more intense pulse, a higher density threshold is required, e.g., $n_{L,21} = 2.5 n_c(\lambda^2/r_0^2)$ for $I_0 = 10^{21}$ Wcm^{-2}. The validity of $n_{L,21}$ is confirmed by our PIC simulations, which reveal that, when n_e is taken as a few of $n_{L,21}$, the pulses with $r_0 = 8$, 16 and 32λ start to self-focus at the beginning stage, and then they attenuate fast due to light absorption in relatively high density plasmas.

5. Summary

In summary, we have shown that there is an upper limit of the laser power P_u for self-focusing in plasma, which is a function of the initial spot size of the laser pulse and the plasma electron density. Self-focusing occurs only when the laser power is above P_u. Otherwise, the laser pulse experiences ponderomotive defocusing due to expulsion of local plasma electrons by the transverse ponderomotive force. It is also found that there is a lower limit of the plasma density n_L for self-focusing, below which self-focusing does not occur for any laser power. These are verified by 2D PIC simulations. The present study provides guidance for future experimental designs when the self-guided propagation of laser pulses over a long distance is required, such as in laser wakefield acceleration with laser power at the 100 TW level or above.

Acknowledgements

This work is supported in part by NSFC (Grant Nos. 11105217, 11121504, and 10925421), National Basic Research Program of China (Grant No. 2009GB105002). Numerical simulations have been partially carried out on 'Magic Cube' at Shanghai Supercomputer Center.

References

1. M. Tabak, J. Hammer, M. Glinsky, W. Kruer, S. Wilks, J. Woodworth, E. Campbell, M. Perry, and R. Mason, Phys. Plasmas **1**, 1628 (1994).
2. A. L. Lei, K. A. Tanaka, R. Kodama, K. Adumi, H. Habara, Y. Kitagawa, K. Kondo, T. Matsuoka, T. Tanimoto, T. Yabuuchi, K. Mima, K. Nagai, H. Nagatomo, T. Norimatsu, K. Sawai, K. Suzuki, Wei Yu, Han Xu, X. Q. Yang, L. H. Cao, H. B. Cai, Y. Sentoku, A. Pukhov, R. Kumar, R. Snavely, R. Freeman, Min Yu, and J. Zheng, Phys. Plasmas **16**, 056307 (2009).
3. T. Tajima, and J. M. Dawson, Phys. Rev. Lett. **43**, 267 (1979).
4. E. Esarey, C. B. Schroeder, and W. P. Leemans, Rev. Mod. Phys. **81**, 1229 (2009).
5. S. P. D. Mangles, C. D. Murphy, Z. Najmudin, A. G. R. Thomas, J. L. Collier, A. E. Dangor, E. J. Divall, P. S. Foster, J. G. Gallacher, C. J. Hooker, D. A. Jaroszynski, A. J. Langley, W. B. Mori, P. A. Norreys, F. S. Tsung, R. Viskup, B. R. Walton, and K. Krushelnick, Nature (London) **431**, 535 (2004); C. Geddes, C. Toth, J. van Tilborg, E. Esarey, C. Schroeder, D. Bruhwiler, C. Nieter, J. Cary, and W. Leemans, Nature (London) **431**, 538 (2004); J. Faure, Y. Glinec, A. Pukhov, S. Kiselev, S. Gordienko, E. Lefebvre, J. Rousseau, F. Burgy, and V. Malka, Nature (London) **431**, 541 (2004).
6. J. Faure, C. Rechatin, A. Norlin, A. Lifschitz, Y. Glinec, and V. Malka, Nature (London) **444**, 737 (2006).
7. W. P. Leemans, B. Nagler, A. J. Gonsalve, Cs. Tóth, K. Nakamura, C. G. R. Geddes, E. Esarey, C. B. Schroeder, and S. M. Hooker, Nat. Phys. **2**, 696 (2006).
8. W.-M. Wang, Z.-M. Sheng, and J. Zhang, Appl. Phys. Lett. **93**, 201502 (2008); W.-M. Wang and Z.-M. Sheng, Phys. Plasmas **15**, 013101 (2008); W.-M. Wang, Z.-M. Sheng, J. Zhang, Laser Part. Beams **27**, 3 (2009).
9. A. Couairon, and A. Mysyrowicz, Physics Reports **441**, 47 (2007).
10. L. Berge, S. Skupin, R. Nuter, J. Kasparian, and J.-P. Wolf, Rep. Prog. Phys. **70**, 1633 (2007).
11. M. Y. Yu, P. K. Shukla, and K. H. Spatschek, Phys. Rev. A **18**, 1591 (1978).
12. G.-Z. Sun, E. Ott, Y. C. Lee, and P. Guzdar, Phys. Fluids **30**, 526 (1987).
13. P. Sprangle, C. M. Tang, and E. Esarey, IEEE Trans. Plasma Sci. **15**, 145 (1987).
14. A. B. Borisov, A. V. Forovskiy, O. B. Shiryaev, V. V. Korobkin, A. M. Prokhorov, J. C. Solem, T. S. Luk, K. Boyer, and C. K. Rhodes, Phys. Rev. A **45**, 5830 (1992).
15. Z. M. Sheng, K. Nishihara, T. Honda, S. Bulanov, Y. Sentoku, and K. Mima, Phys. Rev. E **64**, 066409 (2001).
16. G. Li, R. Yan, C. Ren, T.-L. Wang, J. Tonge, and W. B. Mori, Phys. Rev. Lett. **100**, 125002 (2008).
17. L. Willingale, P. M. Nilson, A. G. R. Thomas, J. Cobble, R. S. Craxton, A. Maksimchuk, P. A. Norreys, T. C. Sangster, R. H. H. Scott, C. Stoeckl, C. Zulick, and K. Krushelnick, Phys. Rev. Lett. **106**, 105002 (2011).
18. L. M. Chen, H. Kotaki, K. Nakajima, J. Koga, S. V. Bulanov, T. Tajima, Y. Q. Gu, H. S. Peng, X. X. Wang, T. S. Wen, H. J. Liu, C. Y. Jiao, C. G. Zhang, X. J. Huang, Y. Guo, K. N. Zhou, J. F. Hua, W. M. An, C. X. Tang, and Y. Z. Lin, Phys. Plasmas **14**, 040703 (2007).
19. J. Fuchs, E. Humieres, Y. Sentoku, P. Antici, S. Atzeni, H. Bandulet, S. Depierreux, C. Labaune, and A. Schiavi, Phys. Rev. Lett. **105**, 225001 (2010).
20. W.-M. Wang, and C.-Y. Zheng, Phys. Plasmas **13**, 053112 (2006).
21. C. Ren, R. G. Hemker, R. A. Fonseca, B. J. Duda, and W. B. Mori, Phys. Rev. Lett. **85**, 2124 (2000).
22. Q. L. Dong, Z. M. Sheng, and J. Zhang, Phys. Rev. E **66**, 027402 (2002).
23. H.-C. Wu, Z.-M. Sheng, and J. Zhang, Phys. Rev. E **70**, 026407 (2004).
24. T.-T. Xi, X. Lu, and J. Zhang, Phys. Rev. Lett. **96**, 025003 (2006).
25. Z. Wang, C. Liu, Z. Shen, Q. Zhang, H. Teng, and Z. Wei, Opt. Lett. **36**, 3194 (2011).
26. T. Kameshima, W. Hong, K. Sugiyama, X. L. Wen, Y. C. Wu, C. M. Tang, Q. H. Zhu, Y. Q. Gu, B. H. Zhang, H. S. Peng, S. Kurokawa, L. M. Chen, T. Tajima, T. Kumita, and K. Nakajima, Appl. Phys. Exp. **1**, 066001 (2008).
27. W. P. Leemans, B. Nagler, A. J. Gonsalve, Cs. Toth, K. Nakamura, C. G. R. Geddes, E. Esarey, C. B. Schroeder, and S. M. Hooker, Nat. Phys. **2**, 696 (2006).
28. J. S. Liu, C. Q. Xia, W. T. Wang, H. Y. Lu, Ch. Wang, A. H. Deng, W. T. Li, H. Zhang, X. Y. Liang, Y. X. Leng, X. M. Lu, C. Wang, J. Z. Wang, K. Nakajima, R. X. Li, and Z. Z. Xu, Phys. Rev. Lett. **107**, 035001 (2011).
29. N. A. M. Hafz, T. M. Jeong, I. W. Choi, S. K. Lee, K. H. Pae, V. V. Kulagin, J. H. Sung, T. J. Yu, K.-H. Hong, T. Hosokai, J. R. Cary, D.-K. Ko, and J. Lee, Nat. Photonics **2**, 571 (2008).
30. W.-M. Wang, Z.-M. Sheng, M. Zeng, Y. Liu, Z.-D. Hu, S. Kawata, C.-Y. Zheng, W. B. Mori, L.-M. Chen, Y.-T. Li, and J. Zhang, Appl. Phys. Lett. **101**, 184104 (2012).
31. J. Meyer-ter-Vehn, A. Pukhov, and Z.-M. Sheng, in *Atoms, Solids, and Plasmas in Super-Intense Laser Fields*, D. Batani, *et al.* eds. (Kluwer Academic/Plenum Publishers 2001), pp. 167–192.
32. W.-M. Wang, Z.-M. Sheng, Y.-T. Li, L.-M. Chen, S. Kawata, and J. Zhang, Phys. Rev. ST Accel. Beams **13**, 071301 (2010).
33. K.-C. Tzeng, and W. B. Mori, Phys. Rev. Lett. **81**, 104 (1998).
34. C. D. Decker, W. B. Mori, K.-C. Tzeng, and T. C. Katsouleas, IEEE Trans. Plasma Sci. **24**, 379 (1996).
35. W. Lu, M. Tzoufras, C. Joshi, F. S. Tsung, W. B. Mori, J. Vieira, R. A. Fonseca, and L. O. Silva, Phys. Rev. ST Accel. Beams **10**, 061301 (2007).
36. S. Gordienko, and A. Pukhov, Phys. Plasmas **12**, 043109 (2005).